Quasi-Static Surface-PEEC Modeling of Electromagnetic Problem With Finite Dielectrics

Yang Jiang and Ke-Li Wu, *Fellow, IEEE*

***Abstract*— This paper presents a quasi-static surface-based partial element equivalent circuit (PEEC) model for electromagnetic problems consisting of coupled conductors and heterogeneous dielectrics of finite size. The PEEC model is based on the surface equivalent principle. Unlike the traditional surface-based PEEC models, in which the integral equations are set up by enforcing the field continuity in the true field region, the homogeneous integral equations in this model are obtained by enforcing the tangential null field condition in the null field regions. Simplified integral equations are obtained under the quasi-static assumption, in which the circuit elements carrying electric currents and magnetic charges on the dielectric surfaces are vanished. Consequently, the size of the subcircuit describing dielectrics is reduced significantly compared to the full-wave surface-PEEC (S-PEEC) model. Since the quasi-static S-PEEC model only contains frequency-independent circuit elements, it can be conveniently used for time-domain simulation. Three numerical examples are presented to validate the new PEEC model for typical embedded RF passive components, packaging and interconnection problems in both the frequency domain and the time domain. Excellent agreement is observed between the results of the proposed PEEC model, S-PEEC model, and those of commercial software within the quasi-static frequency range.**

***Index Terms*— Dielectrics, embedded passives, integral equations, interconnection, partial element equivalent circuit (PEEC) method.**

I. Introduction

MODERN electronic packaging for high-speed and high-frequency systems involves high density conductor routings and heterogeneous dielectrics of finite size. An accurate and effective modeling of the complex electromagnetic (EM) phenomena involved in the packaging structures is critical in the design stage of a high-performance package and circuit. It is highly desirable that the modeling can not only predicate the frequency domain but also the time-domain responses effectively.

Among various modeling methods, the partial element equivalent circuit (PEEC) method [1]–[6] is the only method that can convert an EM problem into a circuit domain representation that can be analyzed in both frequency and time domains using a circuit solver. In recent years, the PEEC model also serves as a starting point to derive a concise physically meaningful circuit [7]–[10] that can accelerate signal integrity analysis of a layered media problem significantly.

To model an EM problem involving heterogeneous dielectrics of finite size based on the concept of PEEC modeling, the volume and surface equivalence principles have been adopted in developing a volume-PEEC (or V-PEEC) [2] and a surface-PEEC (or S-PEEC) [3], respectively. Compared with the V-PEEC in [2], the S-PEEC is more efficient and accurate when handling a problem involving heterogeneous dielectrics, which is the most commonly seen scenario in electronic packaging. The S-PEEC introduces two sets subcircuits on dielectric surfaces, one comes from the electric field integral equation (EFIE) and the other is derived from the magnetic field integral equation (MFIE). Each subcircuit consists of a mesh-dependent circuit involving inductors, capacitors, and mutual couplings among the inductive elements and capacitive elements. The basic configuration of each subcircuit is the same as that for a multiple conductor problem [1]. In addition, mixed types of couplings among the two sets of subcircuits reflect the electric field generated by the magnetic current and the magnetic field generated by the electric current. All the currents are assumed to flow on the surfaces of the dielectrics and conductors.

In fact, for most of electronic packaging problems, their electrical size is very small and the radiation effect is negligible, to which the effectiveness of the quasi-static approximation can be easily justified. The approximation has been successfully used in modeling of embedded passives and signal integrity analysis [11]–[14]. To handle heterogeneous dielectrics of finite size, a PEEC method based on the volume equivalence principle under quasi-static approximation was proposed in [13]. However, for the problem with arbitrary shape finite heterogeneous dielectrics a quasi-static S-PEEC model would be very effective but is not available. Conceptually, in such quasi-static model, the contributions from the insignificant equivalent current and charge, namely, the electric current and magnetic charge on the surfaces of dielectrics, can be naturally ignored. This paper is an attempt toward this direction, aiming at a much simpler but more efficient S-PEEC model under quasi-static approximation.

In the proposed new PEEC model, the surface equivalence principle is utilized to establish the essential EFIE and MFIE equations. The quasi-static approximation is applied to the two sets of equations before they are merged in a legitimate way. Three general integral equations, namely, an EFIE for

Manuscript received June 20, 2018; revised August 31, 2018 and October 13, 2018; accepted October 24, 2018. Date of publication December 11, 2018; date of current version February 5, 2019. This work was supported by the Research Grants Council of the Hong Kong Special Administrative Region, China, under Grant AoE/P-04/08. *(Corresponding author: Ke-Li Wu.)*

The authors are with the Department of Electronic Engineering, The Chinese University of Hong Kong, Hong Kong (e-mail: yjiang@ee.cuhk.edu.hk; klwu@cuhk.edu.hk).

Color versions of one or more of the figures in this paper are available online at http://ieeexplore.ieee.org.

Digital Object Identifier 10.1109/TMTT.2018.2882481

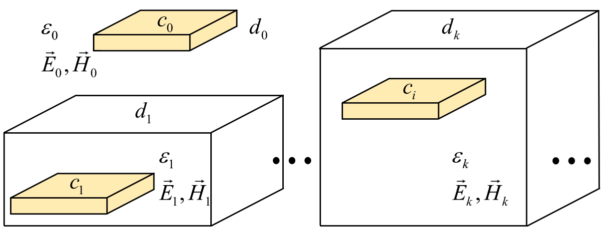

Fig. 1. Conductors and dielectrics under consideration.

conductors, an MFIE, and an EFIE for dielectrics, are obtained by analytic derivation. The three equations lead to the new PEEC model with the following three attractive features.

1) The circuit elements carrying the equivalent electric current and magnetic charge on the dielectric surfaces are eliminated. As a result, the number of circuit elements related to dielectric surfaces is reduced nearly by half compared to the existing full-wave S-PEEC model.
2) Only capacitive circuit elements on the dielectric surfaces exist, reflecting the nature of the induced charge on dielectric surfaces in a quasi-statistic field. The capacitive elements are turned to be open circuited when the permittivity of the dielectric approaches that of the surrounding background. This feature ensures that the new PEEC model works well when the permittivity of the dielectric is close to that of free space.
3) All the circuit elements are frequency independent so that the S-PEEC model can be conveniently used for the time-domain simulation.

The aforementioned features can significantly reduce the modeling time and required memory usage because the number of unknowns is reduced and the circuit coupling matrix is sparser compared to the traditional S-PEEC.

This paper is organized as follows. In Section II, the integral equations based on the surface equivalence principle are developed. Section III presents three new integral equations that are formulated based on the surface equivalence principle under quasi-static approximation. Section IV shows that having applied the discretization and matching processes to the three integral equations a clear circuit interpretation of the EM problem can be given. Three numerical examples are given to validate the proposed new S-PEEC model. The numerical results obtained by the model are compared with those obtained by commercial EM software and the existing PEEC models in Section V, followed by discussions and conclusions in Section VI.

II. Surface Equivalence Principle

The surface equivalence principle states that an EM problem can be modeled by interior and exterior region problems by introducing surface equivalent sources. Considering an EM problem that comprises N dielectrics and $N+1$ conductors, as illustrated in Fig. 1, where $\{c_0, c_1, \ldots c_k, \ldots, c_N\}$ are conductors embedded in background d_0 and dielectrics $\{d_1, \ldots d_k, \ldots, d_N\}$, which are with permittivity ε_0 and $\{\varepsilon_1, \ldots, \varepsilon_k, \ldots \varepsilon_N\}$, respectively. Surfaces

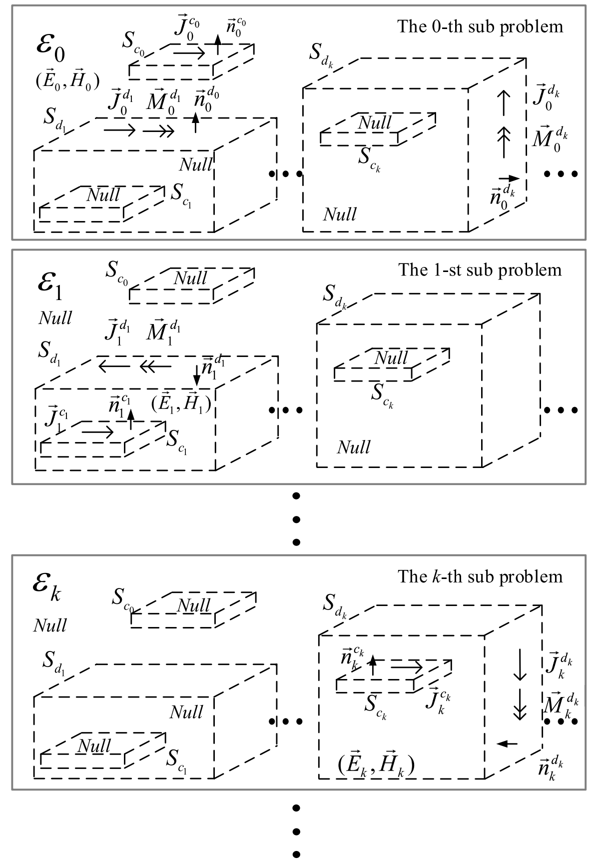

Fig. 2. $N+1$ equivalent subproblems.

$\{S_{d_0}, S_{d_1}, \ldots S_{d_k}, \ldots, S_{d_N}\}$ refer to the $N+1$ closed surfaces of the background and dielectrics $\{d_1, \ldots d_k, \ldots, d_N\}$, respectively. Surfaces $\{S_{c_0}, S_{c_1}, \ldots S_{c_k}, \ldots, S_{c_N}\}$ refer to the surfaces of the $N+1$ conductors, respectively. Applying the surface equivalence principle to the background region and each homogeneous dielectric region one by one by retaining the true field inside each region and setting the null field elsewhere, the original EM problem is divided into $N+1$ subproblems, as shown in Fig. 2. In the ith subproblem, the whole space is filled up by the dielectric with permittivity ε_i. The EM field inside surface S_{d_i} is the true field but outside of the surface is null. According to the surface equivalence principle, such a field arrangement is supported by the equivalent surface sources

$$\vec{J}_i^{d_i} = \vec{n}_i^{d_i} \times \vec{H} \qquad \vec{M}_i^{d_i} = \vec{E} \times \vec{n}_i^{d_i} \tag{1}$$

on S_{d_i}, and

$$\vec{J}_i^{c_i} = \vec{n}_i^{c_i} \times \vec{H} \tag{2}$$

on S_{c_i}, where $\vec{n}_i^{d_i, c_i}$ is the normal unit vector pointing to the true field region. Obviously, the equivalent sources on the two sides of the same dielectric surafce are related by

$$\vec{J}_0^{d_i} = -\vec{J}_i^{d_i}, \quad \vec{M}_0^{d_i} = -\vec{M}_i^{d_i}. \tag{3}$$

The EM fields $(\vec{E}_i, \vec{H}_i)$ in the ith subproblem $(i = 0, 1, \ldots, N)$ can be expressed by potential functions in a homogeneous space filled with dielectric (ε_i, μ_0) by

$$\vec{E}_i(r) = -j\omega\vec{A}_i(r) - \nabla\Phi_i(r) - \nabla \times \frac{1}{\varepsilon_i}\vec{F}_i(r) \tag{4}$$

$$\vec{H}_i(r) = -j\omega\vec{F}_i(r) - \nabla\varphi_i(r) + \nabla \times \frac{1}{\mu_0}\vec{A}_i(r) \tag{5}$$

in which ω is the angular frequency. The electric vector potential function $\vec{A}_i$, the magnetic vector potential function $\vec{F}_i$, the electric scalar potential function ϕ_i, and the magnetic scalar potential function φ_i for the ith subproblem can be found by

$$\vec{A}_i(r) = \mu_0 \int G_i(r,r')\vec{J}_i(r')ds' \tag{6a}$$

$$\vec{F}_i(r) = \varepsilon_i \int G_i(r,r')\vec{M}_i(r')ds' \tag{6b}$$

$$\Phi_i(r) = \frac{1}{\varepsilon_i}\int G_i(r,r')\rho_i(r')ds' \tag{6c}$$

$$\varphi_i(r) = \frac{1}{\mu_0}\int G_i(r,r')\sigma_i(r')ds' \tag{6d}$$

where $\vec{J}_i$, $\vec{M}_i$, ρ_i, and σ_i are the equivalent surface density functions of electric current, magnetic current, electric charge, and magnetic charge in the ith subproblem, respectively. $G(r,r')$ is Green's function of a homogeneous medium

$$G_i(r,r') = \frac{\exp(-j\omega\sqrt{\varepsilon_i\mu_0}|r-r'|)}{4\pi|r-r'|}. \tag{7}$$

Under quasi-static assumptation, Green's function in (7) can be approximated by

$$G^Q(r,r') = \frac{1}{4\pi|r-r'|}. \tag{8}$$

III. Integral Equations for Quasi-Static PEEC Model

Define surfaces $\{S^+_{d_0},\ldots,S^+_{d_N}\}$ and $\{S^-_{d_0},\ldots,S^-_{d_N}\}$ as the inner surfaces located in the true field region and the outer surfaces located in the null field region of surfaces $\{S_{d_0},\ldots,S_{d_N}\}$ in the respective subproblems. Obviously, $S^{\pm}_{d_0} = \{S^{\mp}_{d_1},\ldots,S^{\mp}_{d_N}\}$. Surfaces $\{S^+_{c0},\ldots,S^+_{cN}\}$ are the surfaces infinitely close to conductor surfaces $\{S_{c0},\ldots,S_{cN}\}$ in the true field region. In each subproblem, two sets of boundary conditions are utilized to set up required integral equations. One is boundary conditions (9) applied on dielectric surfaces, and the other is (10) applied on conductor surfaces.

On dielectric surfaces, unlike the traditional approach to set up integral equations using the surface equivalent principle, in which the field continuity relation in the true field region is used, the approach in this paper enforces the tangential fields in the null field region to be zero. In the 0th subproblem, the tangential components of $\vec{E}_0(r)$ and $\vec{H}_0(r)$ on the surface $S^-_{d_0}$ are enforced to be zero. For the rest of subproblems, taking the ith subproblem as an example, the tangential components of $\vec{E}_i(r)$ and $\vec{H}_i(r)$ on the surface of every dielectric in the null field region, $S^-_{d_j}$ $(j = 1,\ldots,N)$, are set to zero, i.e.,

$$\vec{E}_i(r)|_{\tan} = 0, \quad \vec{H}_i(r)|_{\tan} = 0$$

$$r \in \begin{cases} S^-_{d_0}, & \text{if } i = 0 \\ S^-_{d_j}(j = 1,\ldots,N), & \text{if } i \neq 0. \end{cases} \tag{9}$$

In addition, in each subproblem, the tangential component of the electric field on surfaces $S^+_{c_j}$ $(j = 0,\ldots,N)$ vanishes in each subproblem, or

$$\vec{E}_i(r)|_{\tan} + \vec{E}^{\text{inc}}_i(r)\big|_{\tan} = 0, \quad r \in S^+_{c_j},\ j = 0,\ldots,N \tag{10}$$

where $i = 0,\ldots,N$, $\vec{E}^{\text{inc}}_i$ is the incident field in region i. The field expressions for $\vec{E}_i(r)$ and $\vec{H}_i(r)$ are given by (4) and (5).

The $N+1$ subproblems introduce $N+1$ integral equations. A set of dedicated integral equations for a quasi-static PEEC model can be acquired by summing up the integral equations for all the $N+1$ subproblems for the same observation point r, including the case in which the observation point is defined by point r^+ or r^- that approach r from either side of the same surface. This summing process leads to

$$\vec{E}_0(r^+)|_{\tan} + \sum_{i=1}^{N}\vec{E}_i(r^-)|_{\tan} = 0 \quad \left(r^{\pm} \in S^{\pm}_{d_j},\ j = 1,\ldots,N\right) \tag{11}$$

$$\vec{H}_0(r^+)|_{\tan} + \sum_{i=1}^{N}\vec{H}_i(r^-)|_{\tan} = 0 \quad \left(r^{\pm} \in S^{\pm}_{d_j},\ j = 1,\ldots,N\right) \tag{12}$$

$$\sum_{i=0}^{N}\vec{E}_i(r)|_{\tan} = -\vec{E}^{\text{inc}}_i(r)\big|_{\tan} \quad \left(r \in S^+_{c_j},\ j = 0,\ldots,N\right). \tag{13}$$

The superscripts "+" and "−" of observation point r in (11) and (12) represent the two points that approach r from the two sides of the same dielectric surface. Reminded that $S^-_{d_0} = \{S^+_{d_1},\ldots,S^+_{d_N}\}$, r^+ in (11) and (12) is the same as r defined in (9) in the 0th subproblem. Substituting (6) into (11)–(13) leads to the following integral equations, respectively,

$$\Bigg[-j\omega\vec{A}_0(r^+) - \nabla\Phi_0(r^+) - \nabla \times \frac{1}{\varepsilon_0}\vec{F}_0(r^+) - j\omega\sum_{i=1}^{N}\vec{A}_i(r^-) - \nabla\sum_{i=1}^{N}\Phi_i(r^-) - \nabla\times\sum_{i=1}^{N}\frac{1}{\varepsilon_i}\vec{F}_i(r^-)\Bigg]_{\tan} = 0 \tag{14}$$

$$\Bigg[-j\omega\vec{F}_0(r^+) - \nabla\varphi_0(r^+) + \nabla \times \frac{1}{\mu_0}\vec{A}_0(r^+) - j\omega\sum_{i=1}^{N}\vec{F}_i(r^-) - \nabla\sum_{i=1}^{N}\varphi_i(r^-) + \nabla\times\sum_{i=1}^{N}\frac{1}{\mu_i}\vec{A}_i(r^-)\Bigg]_{\tan} = 0 \tag{15}$$

$$\Bigg[-j\omega\sum_{i=0}^{N}\vec{A}_i(r) - \nabla\sum_{i=0}^{N}\Phi_i(r) - \nabla\times\sum_{i=0}^{N}\frac{1}{\varepsilon_i}\vec{F}_i(r)\Bigg]_{\tan} = -\vec{E}^{\text{inc}}_i(r)\big|_{\tan}. \tag{16}$$

The summations of potential functions in (14)–(16) can be simplified under quasi-static assumption in Section III-A, III-B, and III-C.

A. Summations of Vector Potential Functions

The summation of the electric vector potentials $\vec{A}_0 + \Sigma \vec{A}_i$ can be simplified by replacing Green's function in (6a) by its quasi-static approximation (8), i.e.,

$$\begin{aligned}\vec{A}_0(r^+) &+ \sum_{i=1}^{N} \vec{A}_i(r^-) \\ &= \mu_0 \int_{S_{d_0}, S_{c_0}} G^Q(r^+, r')\vec{J}_0(r')ds' \\ &\quad + \mu_0 \sum_{i=1}^{N} \int_{S_{d_i}, S_{c_i}} G^Q(r^-, r')\vec{J}_i(r')ds'. \end{aligned} \tag{17}$$

Since the vector potentials under quasi-static approximation are continues across a dielectric surface and that the field points r^+ and r^- are infinitely close to r, (17) can be rewritten as

$$\begin{aligned}\mu_0 &\int_{S_{d_0}, S_{c_0}} G^Q(r^+, r')\vec{J}_0(r')ds' \\ &\quad + \mu_0 \sum_{i=1}^{N} \int_{S_{d_i}, S_{c_i}} G^Q(r^-, r')\vec{J}_i(r')ds' \\ &= \mu_0 \int_{S_{d_0}, S_{c_0}} G^Q(r, r')\vec{J}_0(r')ds' \\ &\quad + \mu_0 \sum_{i=1}^{N} \int_{S_{d_i}, S_{c_i}} G^Q(r, r')\vec{J}_i(r')ds'. \end{aligned} \tag{18}$$

Notice that the electric current exists on the surfaces of both conductors and dielectrics. According to (1), $\vec{J}_0$ can be reexpressed in terms of the currents on dielectric surfaces S_{d_i} ($i = 1, \ldots, N$) and on conductor surface S_{c_0}. The electric current for the ith subproblem $\vec{J}_i$ consists of two parts: the electric current on the surface of dielectric d_i and on the surface of conductor c_i. That is to say

$$\vec{J}_0(r') = \sum_{i=1}^{N} \vec{J}_0^{d_i}(r') + \vec{J}_0^{c_0}(r'), \quad \vec{J}_i(r') = \vec{J}_i^{d_i}(r') + \vec{J}_i^{c_i}(r') \tag{19}$$

where the subscript "0" or "i" refers to the case in which the field in region 0 or i is the true field. Replacing the electric current density in (18) by (19) leads to

$$\begin{aligned}\vec{A}_0(r^+) &+ \sum_{i=1}^{N} \vec{A}_i(r^-) \\ &= \mu_0 \int_{S_{d_0}} G^Q(r, r') \sum_{i=1}^{N} \vec{J}_0^{d_i}(r')ds' \\ &\quad + \mu_0 \int_{S_{c_0}} G^Q(r, r')\vec{J}_0^{c_0}(r')ds' \\ &\quad + \sum_{i=1}^{N} \mu_0 \int_{S_{d_i}} G^Q(r, r')\vec{J}_i^{d_i}(r')ds' \\ &\quad + \sum_{i=1}^{N} \mu_0 \int_{S_{c_i}} G^Q(r, r')\vec{J}_i^{c_i}(r')ds'. \end{aligned} \tag{20}$$

Noted that $S_{d_0} = \{S_{d_1}, \ldots, S_{d_N}\}$. By rearranging the summation in (20), the following equation can be obtained:

$$\begin{aligned}\vec{A}_0(r^+) &+ \sum_{i=1}^{N} \vec{A}_i(r^-) \\ &= \sum_{i=1}^{N} \mu_0 \int_{S_{d_i}} G^Q(r, r')\big[\vec{J}_0^{d_i}(r') + \vec{J}_i^{d_i}(r')\big]ds' \\ &\quad + \sum_{i=0}^{N} \mu_0 \int_{S_{c_i}} G^Q(r, r')\vec{J}_i^{c_i}(r')ds'. \end{aligned} \tag{21}$$

Using (3), the first term on the right-hand side (RHS) of (21) equals to zero, which means that the summation of the electric vector potential only depends on the electric current on the surfaces of conductors, such that

$$\begin{aligned}\vec{A}_0(r^+) + \sum_{i=1}^{N} \vec{A}_i(r^-) &= \sum_{i=0}^{N} \mu_0 \int_{S_{c_i}} G^Q(r, r')\vec{J}_i^{c_i}(r')ds' \\ &= \mu_0 \int_{S_c} G^Q(r, r')\vec{J}(r')ds' \end{aligned} \tag{22}$$

where $S_c = \{S_{c0}, S_{c_1}, \ldots, S_{cN}\}$. Similarly, the summation of magnetic vector potential $\vec{F}_0 + \Sigma \vec{F}_i$ can be simplified as

$$\begin{aligned}\vec{F}_0(r^+) &+ \sum_{i=1}^{N} \vec{F}_i(r^-) \\ &= \varepsilon_0 \int_{S_{d_0}} G^Q(r^+, r') \sum_{i=1}^{N} \vec{M}_0^{d_i}(r')ds \\ &\quad + \sum_{i=1}^{N} \varepsilon_i \int_{S_{d_i}} G^Q(r^-, r')\vec{M}_i^{d_i}(r')ds' \\ &= \sum_{i=1}^{N} \int_{S_{d_i}} G^Q(r, r')\big[\varepsilon_0 \vec{M}_0^{d_i}(r') + \varepsilon_i \vec{M}_i^{d_i}(r')\big]ds' \\ &= \int_{S_d} [\varepsilon_0 - \varepsilon(r')]G^Q(r, r')\vec{M}(r')ds' \end{aligned} \tag{23}$$

in which $S_d = \{S_{d_1}, \ldots, S_{d_N}\}$, $\varepsilon(r')$ is the permittivity of the dielectric on whose surface the sources are introduced, and ε_0 is the permittivity of the background.

B. Gradient of Summations of Scalar Potential Functions

Using the current continuity equation and (3), it can be shown that the equivalent charge densities on the both sides of a dielectric surface satisfy the following properties:

$$\rho_0^{d_i} = -\rho_i^{d_i} \qquad \sigma_0^{d_i} = -\sigma_i^{d_i} \tag{24}$$

in which $i = \{1, \ldots, N\}$.

Considering the gradient of summation of the scalar potentials on the left-hand side (LHS) of (14)–(16), $\nabla\phi_0 + \nabla\Sigma\phi_i$ and $\nabla\varphi_0 + \nabla\Sigma\varphi_i$, the summation can be separated into two terms, the singular and nonsingular terms. The singular term appears when observation point is infinitely close to a source point. As r in (14)–(16) is situated on a conductor or dielectric surface, assuming r^+ and r^- approach a source point that is located at the center of S_δ, an infinitely small circular disk on S_{d_j}, the gradient can be written as

$$\begin{aligned}
&\nabla\Phi_0(r^+) + \nabla\sum_{i=1}^{N}\Phi_i(r^-)\\
&\quad= \frac{1}{\varepsilon_0}\int_{S_\delta}\nabla G^Q(r^+,r')\rho_0^{d_j}(r')ds'\\
&\qquad+\frac{1}{\varepsilon_j}\int_{S_\delta}\nabla G^Q(r^-,r')\rho_j^{d_j}(r')ds'\\
&\qquad+\int_{S_{c_0},S_{d_0}-S_\delta}\nabla G^Q(r^+,r')\rho_0^{d_j}(r')ds'\\
&\qquad+\sum_{i=1}^{N}\frac{1}{\varepsilon_i}\int_{S_{c_i},S_{d_i}-S_\delta}\nabla G^Q(r^-,r')\rho_i(r')ds'. \qquad (25)
\end{aligned}$$

The first and second terms on the RHS of (25) are the singular integrals. It can be proved that the tangential component of the singular integrals approaches zero [15]. With (24), it can be shown that the tangential components of the nonsingular terms in (25) can be combined in a similar way as that in (23), such that

$$\begin{aligned}
&\frac{1}{\varepsilon_0}\int_{S_{c_0},S_{d_0}-S_\delta}\nabla G^Q(r^+,r')\rho_0(r')ds'\\
&\qquad+\sum_{i=1}^{N}\frac{1}{\varepsilon_i}\int_{S_{d_i},S_{c_i}-S_\delta}\nabla G^Q(r^-,r')\rho_i(r')ds'\\
&\quad=\sum_{i=0}^{N}\int_{S_{c_i}}\frac{1}{\varepsilon_i}\nabla G^Q(r,r')\rho_i^{c_i}(r')ds'\\
&\qquad+\sum_{i=1}^{N}\int_{S_{d_i}-S_\delta}\nabla G^Q(r,r')\left[\frac{\rho_0^{d_i}(r')}{\varepsilon_0}+\frac{\rho_i^{d_i}(r')}{\varepsilon_i}\right]ds'\\
&\quad=\int_{S_c}\frac{1}{\varepsilon(r')}\nabla G^Q(r,r')\rho(r')ds'\\
&\qquad+\int_{S_d-S_\delta}\nabla G^Q(r,r')\left[\frac{1}{\varepsilon_0}-\frac{1}{\varepsilon(r')}\right]\rho(r')ds'. \qquad (26)
\end{aligned}$$

In summary, the tangential component of the gradient of the summation of the electric scalar potential can be written as

$$\begin{aligned}
&\left[\nabla\Phi_0(r^+)+\nabla\sum_{i=1}^{N}\Phi_i(r^-)\right]_{\tan}\\
&\quad=\left\{\int_{S_c}\nabla G^Q(r,r')\frac{\rho(r')}{\varepsilon(r')}ds'+\int_{S_d}\nabla G^Q(r,r')\right.\\
&\qquad\left.\times\left[\frac{1}{\varepsilon_0}-\frac{1}{\varepsilon(r')}\right]\rho(r')ds'\right\}_{\tan}\\
&\quad=\nabla\left\{\int_{S_c}G^Q(r,r')\frac{\rho(r')}{\varepsilon(r')}ds'+\int_{S_d}G^Q(r,r')\right.\\
&\qquad\left.\times\left[\frac{1}{\varepsilon_0}-\frac{1}{\varepsilon(r')}\right]\rho(r')ds'\right\}_{\tan}. \qquad (27)
\end{aligned}$$

The tangential component of $\nabla\Phi_0+\nabla\Sigma\Phi_i$ can be proved to be zero because

$$\begin{aligned}
&\left[\nabla\varphi_0(r^+)+\nabla\sum_{i=1}^{N}\varphi_i(r^-)\right]_{\tan}\\
&\quad=\frac{1}{\mu_0}\sum_{i=1}^{N}\int_{S_d}\nabla G^Q(r,r')\left[\sigma_0^{di}(r')+\sigma_i^{di}(r')\right]ds'\Big|_{\tan}=0. \qquad (28)
\end{aligned}$$

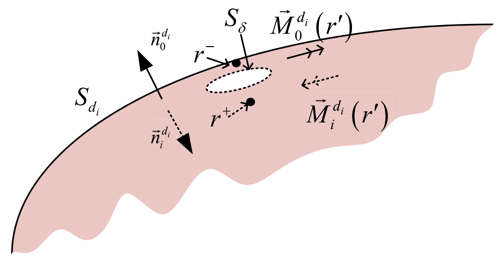

Fig. 3. Observation point in subproblems 0 and j in a singular integral.

The above discussion shows that under the quasi-static approximation the electric charge densities on conductor and dielectric surfaces contribute to the EFIE, whereas the contribution of magnetic charge on dielectric surfaces is null.

C. Curl of Summations of Vector Potential Functions

The third term on the LHS of (14)–(16) involves $\nabla\times\vec{A}_0/\mu_0+\nabla\times\Sigma\vec{A}_i/\mu_0$ and $\nabla\times\vec{F}_0/\varepsilon_0+\nabla\times\Sigma\vec{F}_i/\varepsilon_i$. Taking $\nabla\times\vec{F}_0/\varepsilon_0+\nabla\times\Sigma\vec{F}_i/\varepsilon_i$ as an example, as r^+ and r^- approach a source point located at the center of S_δ on surface S_{d_j}, considering $\vec{M}_0=\sum\vec{M}_0^{di}$, one can find that

$$\begin{aligned}
&\nabla\times\frac{1}{\varepsilon_0}\vec{F}_0(r^+)+\nabla\times\sum_{i=0}^{N}\frac{1}{\varepsilon_i}\vec{F}_i(r^-)\\
&\quad=\int_{S_{d_0}}\nabla G^Q(r^+,r')\times\vec{M}_0(r')ds'\\
&\qquad+\sum_{i=0}^{N}\int_{S_{d_i}}\nabla G^Q(r^-,r')\times\vec{M}_i(r')ds'\\
&\quad=\int_{S_\delta}\nabla G^Q(r^+,r')\times\vec{M}_0^{d_j}(r')ds'\\
&\qquad+\int_{S_\delta}\nabla G^Q(r^-,r')\times\vec{M}_j^{d_j}(r')ds'\\
&\qquad+\int_{S_{d_0}-S_\delta}\nabla G^Q(r^+,r')\times\vec{M}_0(r')ds'\\
&\qquad+\sum_{i=0}^{N}\int_{S_{d_i}-S_\delta}\nabla G^Q(r^-,r')\times\vec{M}_i(r')ds' \qquad (29)
\end{aligned}$$

in which the first and second terms on the RHS are singular and the remaining terms are nonsingular. As shown in Fig. 3, when r^+ and r^- approach S_δ from the both sides of surface S_{d_j}, referring to [15], the singular integrals can be written in the following form:

$$\begin{aligned}
&\int_{S_\delta}\nabla G^Q(r^+,r')\times\vec{M}_0^{d_j}(r')ds'\\
&\qquad+\int_{S_\delta}\nabla G^Q(r^-,r')\times\vec{M}_j^{d_j}(r')ds'\\
&\quad=\frac{\vec{n}_0^{d_j}(r)}{2}\times\vec{M}_0^{d_j}(r)+\frac{\vec{n}_j^{d_j}(r)}{2}\times\vec{M}_j^{d_j}(r)=\vec{n}(r)\times\vec{M}(r) \qquad (30)
\end{aligned}$$

where $\vec{n}$ is the normal unit vector defined in subproblem 0. The nonsingular terms in (29) are continues across a dielectric surface and can be proved to be zero because

$$\begin{aligned}&\int_{S_{d_0}-S_\delta} \nabla G^Q(r^+, r') \times \vec{M}_0(r')ds' \\ &\quad + \sum_{i=1}^{N} \int_{S_{d_i}-S_\delta} \nabla G^Q(r^-, r') \times \vec{M}_i(r')ds' \\ &= \int_{S_{d_0}-S_\delta} \nabla G^Q(r, r') \times \sum_{i=1}^{N} \vec{M}_0^{d_i}(r')ds' \\ &\quad + \sum_{i=1}^{N} \int_{S_{d_i}-S_\delta} \nabla G^Q(r, r') \times \vec{M}_i^{d_i}(r')ds' \\ &= \sum_{i=1}^{N} \int_{S_{d_i}-S_\delta} \nabla G^Q(r, r') \times \left[\vec{M}_0^{d_i}(r') + \vec{M}_i^{d_i}(r')\right]ds' = 0.\end{aligned} \tag{31}$$

In conclusion, combining (30) and (31) into (29) leads to

$$\nabla \times \frac{1}{\varepsilon_0}\vec{F}_0(r^+) + \nabla \times \sum_{i=0}^{N} \frac{1}{\varepsilon_i}\vec{F}_i(r^-) = \vec{n}(r) \times \vec{M}(r). \tag{32}$$

Similarly, the curl of the summation of electric vector potential function in (15) can be found as

$$\begin{aligned}&\nabla \times \frac{1}{\mu_0}\vec{A}_0(r^+) + \nabla \times \sum_{i=0}^{N} \frac{1}{\mu_0}\vec{A}_i(r^-) \\ &\qquad = \int_{S_c} \nabla G^Q(r, r') \times \vec{J}(r')ds' + \vec{n}(r) \times \vec{J}(r).\end{aligned} \tag{33}$$

Equations (32) and (33) indicate that the electric current on conductors contributes to the MFIE, whereas the contribution of the magnetic current to the electric field only exists at the location where the source is.

Substituting (22), (23), (27), (28), (32), and (33) into (14)–(16) one can find three dedicated integral equations. Specifically, they are the EFIE on dielectric surfaces

$$\begin{aligned}\Bigg\{&\nabla \int_{S_c} G^Q \frac{1}{\varepsilon(r')}\rho(r')ds' + \nabla \int_{S_d} G^Q \left[\frac{1}{\varepsilon_0} - \frac{1}{\varepsilon(r')}\right]\rho(r')ds' \\ &+ j\omega\mu_0 \int_{S_c} G^Q \vec{J}(r')ds' + \vec{n}(r) \times \vec{M}(r)\Bigg\}_{\tan} = 0\end{aligned} \tag{34}$$

the MFIE on dielectric surfaces

$$\begin{aligned}\Bigg\{&j\omega \int_{S_d} [\varepsilon(r') - \varepsilon_0] G^Q \vec{M}(r')ds' \\ &+ \int_{S_c} \nabla G^Q \times \vec{J}(r')ds' + \vec{n}(r) \times \vec{J}(r)\Bigg\}_{\tan} = 0\end{aligned} \tag{35}$$

and the EFIE on conductor surfaces

$$\begin{aligned}\Bigg\{&\nabla \int_{S_c} G^Q \frac{1}{\varepsilon(r')}\rho(r')ds' + \nabla \int_{S_d} G^Q \left[\frac{1}{\varepsilon_0} - \frac{1}{\varepsilon(r')}\right]\rho(r')ds' \\ &+ j\omega\mu_0 \int_{S_c} G^Q \vec{J}(r')ds' + \vec{E}_i^{\text{inc}}(r)\Bigg\}_{\tan} = 0.\end{aligned} \tag{36}$$

For simplicity, symbol G^Q represents a short form of quasi-static Green's functions defined in (8). From (34)–(36), one can find that the contributions of magnetic charge density and that of the equivalent electric current on dielectric surfaces are vanished in the integrals under quasi-static assumption. Only the electric current on the surfaces of conductors, the magnetic current on dielectrics surfaces and electric charges take part in the integrals.

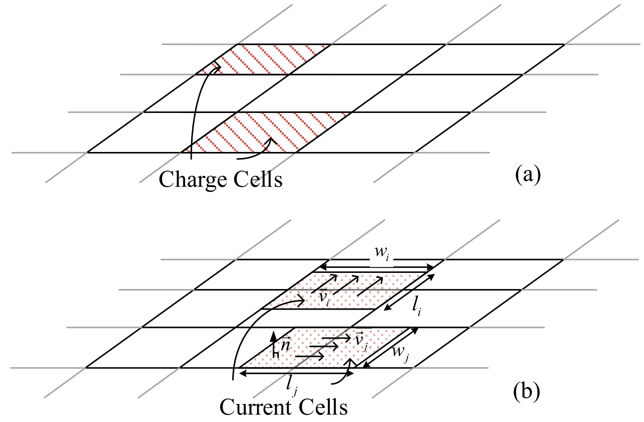

Fig. 4. Surface current and charge cells. (a) Charge cells. (b) ith and jth current cells.

IV. Circuit Domain Interpretation

In this section, a circuit domain interpretation of integral equations (34)–(36) will be given after discretizing and matching procedures. In the same time, the equivalent circuit and corresponding elements are also obtained.

A. Discretization

Even though triangular or quadrilateral mesh cells can be applied to discretize the surfaces, for the clarity, rectangular mesh cells and pulse basis functions are used in this discussion.

Having divided all the dielectric and conductor surfaces by rectangular charge cells, every connected pair of charge cells form a current cell, as shown in Fig. 4, where the width and length of the ith current cell are w_i and l_i, respectively. The distributions of electric and magnetic currents, as well as the electric charge on the surfaces of conductors and dielectrics are discretized by

$$\vec{J}(r) = \sum_{i=1}^{M_c} \vec{b}_i(r)J_i^C + \sum_{j=1}^{M_d} \vec{b}_j(r)J_j^D \tag{37}$$

$$\vec{M}(r) = \sum_{j=1}^{M_d} \vec{c}_j(r)M_j^D \tag{38}$$

$$\rho(r) = \sum_{k=1}^{N_c} f_k(r)\rho_k^C + \sum_{l=1}^{N_d} f_l(r)\rho_l^D \tag{39}$$

in which M_c, M_d, N_c, and N_d denote the total numbers of current cells on conductors and dielectrics, number of charge cells on conductors and dielectrics, respectively. The super-script "C" and "D" of the discretized sources denote the source

TABLE I
DEFINITION OF EQUIVALENT VARIABLES

Variables in Field Domain	Variables in Circuit Domain	Relation
$J_i^{C(D)}$	$I_i^{C(D)}$	$I_i^{C(D)} = w_i J_i^{C(D)}$
M_j^D	V_j^D	$V_j^D = l_j M_j$
$\rho_k^{C(D)}$	$I_k^{C_{Dis}(D_{Dis})}$	$I_k^{C_{Dis}(D_{Dis})} = j\omega A_k \rho_k^{C(D)}$

location on conductor and dielectric surfaces, respectively. The basis functions $\vec{b}_i$, $\vec{c}_j$, and f_k are defined as

$$\vec{b}_i(r) = \begin{cases} \vec{\upsilon}_i, & r \in i\text{th current cell} \\ 0, & \text{otherwise} \end{cases} \tag{40}$$

$$\vec{c}_j(r) = \begin{cases} \vec{\upsilon}_j \times \vec{n}, & r \in j\text{th current cell} \\ 0, & \text{otherwise} \end{cases} \tag{41}$$

$$f_k(r) = \begin{cases} 1, & r \in k\text{th charge cell} \\ 0, & \text{otherwise} \end{cases} \tag{42}$$

where $\vec{\upsilon}_i$ is a unit vector that defines the direction of the tangential current on current cell i, as shown in Fig. 4, and $\vec{n}$ is a unit vector normal to the surface pointing outwards.

For the convenience of discussion, the field domain variables in (37)–(39) are replaced by their corresponding circuit domain variables listed in Table I, where A_k is the area of charge cell k. The current density $J_i^{C(D)}$ are expressed by current $I_i^{C(D)}$ on the ith current mesh on conductors or dielectrics. The charge density $\rho_k^{C(D)}$ is regarded as the displacement current on conductors or dielectrics flows from the kth charge cell to the ground. Considering the unit of magnetic current M_j^D is V/m, a voltage V_j^D is introduced by $V_j^D = l_j M_j^D$ on the jth current mesh on the surfaces of dielectrics. The dedicated integral equations (34)–(36) after discretizing lead to the following discretized integral equations by replacing the sources in the field domain with discretized sources in the circuit domain:

1) Discretized EFIE and MFIE on Dielectrics:

$$\left\{ \nabla\Phi(r) + j\omega \sum_{i=1}^{M_c} \frac{\mu_0}{w_i} \int_{S_i} G^Q \vec{b}_i(r') I_i^C ds' + \vec{n} \times \sum_{j=1}^{M_d} \vec{c}_j(r) \frac{V_j^D}{l_j} \right\}_{\tan} = 0 \tag{43}$$

$$\left\{ j\omega \sum_{j=1}^{M_d} \frac{1}{l_j} \int_{S_j} [\varepsilon(r') - \varepsilon_0] G^Q \vec{c}_j(r') V_j^D ds' + \sum_{i=1}^{M_c} \frac{1}{w_i} \int_{S_i} \nabla G^Q \times \vec{b}_i(r') I_i^C ds' + \vec{n} \times \sum_{j=1}^{M_d} \vec{b}_j(r) \frac{I_j^D}{w_j} \right\}_{\tan} = 0. \tag{44}$$

2) Discretized EFIE on Conductors:

$$\left\{ \nabla\Phi(r) + j\omega \sum_{i=1}^{M_c} \frac{\mu_0}{w_i} \int_{S_i} G^Q \vec{b}_i(r') I_i^C ds' \right\}_{\tan} = 0 \tag{45}$$

in which the first term on the LHS of (43) and (45) is the gradient of summation of electric scalar potentials in (27) after discretizing. The discretized electric scalar potential $\phi(r)$ is given by

$$\begin{aligned} \Phi(r) &= \sum_{i=0}^{N} \Phi_i(r) \\ &= \frac{1}{j\omega} \sum_{k=1}^{N_c} \left[\frac{1}{A_k} \int_{S_k} \frac{1}{\varepsilon(r')} G^Q ds' \right] I_k^{C_{\text{Dis}}} \\ &\quad + \frac{1}{j\omega} \sum_{l=1}^{N_d} \left[\frac{1}{A_l} \int_{S_l} \frac{\varepsilon(r') - \varepsilon_0}{\varepsilon(r')\varepsilon_0} G^Q ds' \right] I_l^{D_{\text{Dis}}}. \end{aligned} \tag{46}$$

B. Matching Procedure

Having had discretization of the coupled integral equations, a matching procedure is applied to (43)–(45) to enforce the coupled equations on each of the current cells with the following projection:

$$\langle \vec{t}, \vec{f} \rangle = \int_{S_t} \vec{t} \cdot \vec{f} ds \tag{47}$$

where integration domain S_t is the surface of the testing cell, $\vec{t}$ is the testing function, and $\vec{f}$ is the discretized integral equations to be matched. The three discretized integral equations to be matched are: 1) EFIE (43) with the observation point on the surfaces of dielectrics; 2) MFIE (44) with the observation point on the surfaces of dielectrics; and 3) EFIE (45) with the observation point on the surfaces of conductors. Taking the pth current cell on dielectric and the qth current cell on conductors as examples in the following discussions.

1) EFIE on Dielectric Surfaces: Applying the matching procedure on (43) with $\vec{t} = \vec{b}_p / w_p$ on the pth dielectric current mesh leads to

$$\begin{aligned} &\frac{1}{w_p} \int_{S_p} \vec{b}_p(r) \cdot \nabla\Phi(r) ds \\ &\quad + j\omega \sum_{i=1}^{M_c} \left[\frac{\mu_0}{w_p w_i} \int_{S_p} \int_{S_i} \vec{b}_p(r) \cdot \vec{b}_i(r') G^Q ds' ds \right] I_i^C \\ &\quad + \frac{1}{w_p} \int_{S_p} \vec{b}_p(r) \cdot \left[\vec{n} \times \sum_{j=1}^{M_d} \vec{c}_j(r) \frac{V_j^D}{l_j} \right] ds = 0. \end{aligned} \tag{48}$$

2) MFIE on Dielectric Surfaces: Applying the matching procedure on (44) with $\vec{t} = \vec{c}_p / l_p$ leads to

$$\begin{aligned} &j\omega \sum_{j=1}^{M_d} \left\{ \frac{1}{l_p l_j} \int_{S_p} \int_{S_i} [\varepsilon(r') - \varepsilon_0] \vec{c}_p(r) \cdot \vec{c}_j(r') G^Q ds' ds \right\} V_j^D \\ &\quad + \sum_{i=1}^{M_c} \left\{ \frac{1}{l_p w_i} \int_{S_p} \int_{S_i} \left[\vec{c}_p(r) \times \vec{b}_i(r') \right] \cdot \nabla G^Q ds' ds \right\} I_i^C \end{aligned}$$

$$+\frac{1}{l_p}\int_{S_p}\vec{c}_p(r)\cdot\sum_{j=1}^{M_d}\left[\vec{n}\times\vec{b}_j(r)\frac{I_j^D}{w_j}\right]ds=0. \tag{49}$$

3) EFIE on Conductor Surfaces: Similar to (48), by setting $\vec{t}=\vec{b}_q/w_q$, after applying the matching process on the qth conductor current mesh, (45) becomes

$$\frac{1}{w_q}\int_{S_q}\vec{b}_q(r)\cdot\nabla\Phi(r)ds + j\omega\sum_{i=1}^{M_c}\left\{\frac{\mu_0}{w_q w_i}\int_{S_q}\int_{S_i}\vec{b}_q(r)\cdot\vec{b}_i(r')G^Q ds'ds\right\}I_i^C=0. \tag{50}$$

The gradient of potential function $\phi(r)$ in (48) and (50) can be approximated by finite difference [1]. By applying vector identify of $\vec{b}\cdot\nabla\phi=\nabla\cdot(\vec{b}\phi)-(\nabla\cdot\vec{b})\phi$, the first term on the LHS of (48) and (50) becomes

$$\begin{aligned}\frac{1}{w_p}\int_{S_p}\vec{b}_p(r)\cdot\nabla\Phi(r)ds &\approx -\left(\frac{1}{A_{p^+}}\int_{S_{p^+}}\Phi(r)ds-\frac{1}{A_{p^-}}\int_{S_{p^-}}\Phi(r)ds\right)\\ &= -(\Phi_{p^+}-\Phi_{p^-})\end{aligned} \tag{51}$$

where the integration domain $S_{p^\pm}$ spans two charge cells associated with current cell p. With (46), the potentials $\phi_{p^\pm}$ can be evaluated by

$$\Phi_{p^\pm}=\frac{1}{j\omega}\left(\sum_{k=1}^{N_c}\frac{1}{A_{p^\pm}A_k}\int_{S_{p^\pm}}\int_{S_k}\frac{1}{\varepsilon(r')}G^Q ds'ds\ I_k^{C_{\text{Dis}}} + \sum_{l=1}^{N_d}\frac{1}{A_{p^\pm}A_l}\int_{S_{p^\pm}}\int_{S_l}\frac{\varepsilon(r')-\varepsilon_0}{\varepsilon(r')\varepsilon_0}G^Q ds'ds I_l^{D_{\text{Dis}}}\right). \tag{52}$$

C. Circuit Domain Interpretation

It is obvious that (48) and (50) can be regarded as two KVL equations and (49) as a KCL equation. The circuit interpretation of each of the equations will be given in the following.

1) EFIE and MFIE on Dielectric Surfaces: Each of the three terms on the LHS of (48) represents a voltage drop across a circuit element. The first term represents potential difference between two adjacent charge cells p^+ and p^- as explained by (51) and (52), in which the node potential $\phi_{p^\pm}$ can be defined by potential coefficients $P^C_{p^\pm k}$ and $P^D_{p^\pm l}$ [16] alone with displacement currents $I_k^{C_{\text{dis}}}$ and $I_l^{D_{\text{dis}}}$ such that

$$\Phi_{p^\pm}=\frac{1}{j\omega}\left(\sum_{k=1}^{N_c}P^C_{p^\pm k}I_k^{C_{\text{Dis}}}+\sum_{l=1}^{N_d}P^D_{p^\pm l}I_l^{D_{\text{Dis}}}\right) \tag{53}$$

where

$$P^C_{p^\pm k}=\frac{1}{A_{p^\pm}A_k}\int_{S_{p^\pm}}\int_{S_k}\frac{1}{\varepsilon(r')}G^Q ds'ds \tag{54}$$

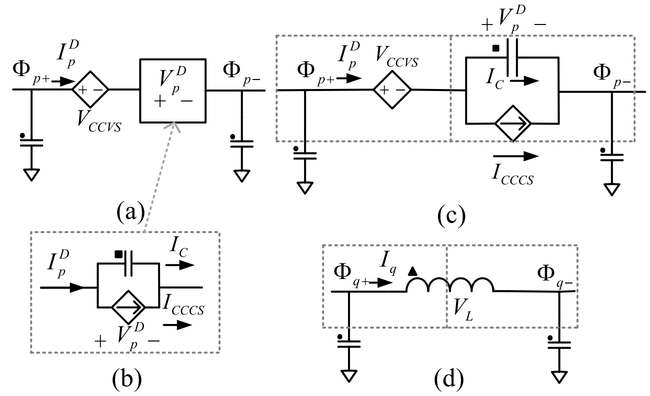

Fig. 5. Circuit interpretation of discretized integral equations. (a) KVL circuit for EFIE on dielectric surfaces. (b) KCL circuit for MFIE on dielectric surfaces. (c) Aggregated circuit on the surface of dielectrics. (d) Circuit on surfaces of conductors.

$$P^D_{p^\pm l}=\frac{1}{A_{p^\pm}A_l}\int_{S_{p^\pm}}\int_{S_l}\frac{\varepsilon(r')-\varepsilon_0}{\varepsilon(r')\varepsilon_0}G^Q ds'ds. \tag{55}$$

The second term is the voltage drop of a current controlled voltage source (CCVS), which can be expressed in terms of circuit domain variables by

$$V_{\text{CCVS}}=j\omega\sum_{i=1}^{M_c}K^{\text{CV}}_{pi}I_i^C \tag{56}$$

where the scaling factor K^{CV}_{pi} is given by

$$K^{\text{CV}}_{pi}=\frac{\mu_0}{w_p w_i}\int_{S_p}\int_{S_i}\vec{b}_p(r)\cdot\vec{b}_i(r')G^Q ds'ds \tag{57}$$

and the third term on the LHS of (48) actually is a local voltage V_p^D introduced by the equivalent magnetic current on a dielectric surface, as defined in Table I. Replacing the basis functions by (40) and (41), one can find that

$$\begin{aligned}\frac{1}{w_p}\int_{S_p}\vec{b}_p(r)\cdot\left[\vec{n}\times\sum_{j=1}^{M_d}\vec{c}_j(r)\frac{V_j^D}{l_j}\right]ds &= \frac{1}{w_p l_p}\int_{S_p}\vec{v}_p\cdot[\vec{n}\times(\vec{v}_p\times\vec{n})]dsV_p^D\\ &=\left(\frac{A_p}{w_p l_p}\right)V_p^D\\ &= V_p^D.\end{aligned} \tag{58}$$

As shown in Fig. 5(a), (48) can be represented by the voltage loop equation $-(\phi_{p^+}-\phi_{p^-})+V_{\text{CCVS}}+V_p^D=0$.

In contrast, (49) can be interpreted as the current node equation $I_C+I_{\text{CCCS}}-I_p^D=0$ from the KCL point of view, as illustrated in Fig. 5(b). The first term on the LHS of (49) stands for the currents through self- and mutual-capacitive couplings, or

$$I_C=j\omega\sum_{j=1}^{M_d}C_{pj}V_j^D \tag{59}$$

with

$$C_{pj}=\frac{1}{l_p l_j}\int_{S_p}\int_{S_i}[\varepsilon(r')-\varepsilon_0]\vec{c}_p(r)\cdot\vec{c}_j(r')G^Q ds'ds \tag{60}$$

where C_{pp} is defined as the self-capacitance on the pth current cell and V_p^D is the voltage across a self-capacitor. The second term on the LHS of (49) is the current induced by a current controlled current source (CCCS), namely, K_{pi}^{CC}, which can be expressed as

$$I_{CCCS} = \sum_{i=1}^{M_c} K_{pi}^{CC} I_i^C \tag{61}$$

with scaling factor

$$K_{pi}^{CC} = \frac{1}{l_p w_i} \int_{S_p} \int_{S_i} [\vec{c}_p(r) \times \vec{b}_i(r')] \cdot \nabla G^Q ds' ds. \tag{62}$$

The third term is regarded as an equivalent current I_p^D because

$$\frac{1}{l_p} \int_{S_p} \vec{c}_p(r) \cdot \sum_{j=1}^{M_d} \left[\vec{n} \times \vec{b}_j(r) \frac{I_j^D}{w_j} \right] ds = \frac{1}{w_p l_p} \int_{S_p} [\vec{v}_p \times \vec{n}] \cdot [\vec{n} \times \vec{v}_p] ds I_p^D = -I_p^D. \tag{63}$$

Considering the partial element circuits shown in Fig. 5(a) and (b), on pth dielectric current cell, the current through the branch, as stated by (49), equals to the current through the self-capacitance alone with other couplings. The voltage across the self-capacitance defined in (60) equals to the voltage between the two ends of the box in Fig. 5(a). Consequently, the whole picture of the PEEC can be obtained by replacing the box in Fig. 5(a) by the circuit in Fig. 5(b), as shown in Fig. 5(c). It should be noticed that when the permittivity of a dielectric approach that of the surrounding background, the value of capacitances given by (60) and the potential coefficient (55), which are the dominant elements on dielectrics, approach zero. In other words, the PEECs on dielectrics naturally become open circuited.

2) EFIE on Conductor Surface: Similar to the EFIE on dielectric surfaces, (50) is regarded as the voltage loop equation $-(\phi_{q^+} - \phi_{q^-}) + V_L = 0$ on the qth current mesh [1], in which

$$\Phi_{q^\pm} = \frac{1}{j\omega} \left(\sum_{k=1}^{N_c} P_{q^\pm k}^C I_k^{C_{\text{Dis}}} + \sum_{l=1}^{N_d} P_{q^\pm l}^D I_l^{D_{\text{Dis}}} \right) \tag{64}$$

$$V_L = j\omega \sum_{i=1}^{M_c} L_{qi} I_i^C \tag{65}$$

where the self- and mutual-inductances L_{qi} between current elements q and i are defined by

$$L_{qi} = \frac{\mu_0}{w_q w_i} \int_{S_q} \int_{S_i} \vec{b}_q(r) \cdot \vec{b}_i(r') G^Q ds' ds. \tag{66}$$

D. Circuit Matrices

Having derived the S-PEEC model, the circuit matrix of the model can be expressed as follows.

1) For the circuit on conductor surfaces

$$[V_S] + [\delta V^C] = j\omega[L][I^C]. \tag{67}$$

2) For the circuit on dielectric surfaces

$$[\delta V^D] = j\omega[K^{CV}][I^C] + [V^D] \tag{68}$$

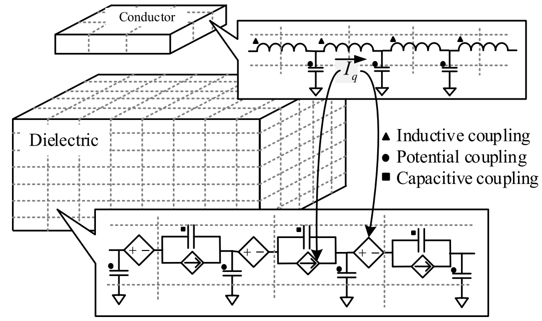

Fig. 6. Quasi-static S-PEEC model for EM problems with conductors and dielectrics.

$$[I^D] = j\omega[C][V^D] + [K^{CC}][I^C] \tag{69}$$

and the node potentials are related to displacement currents by

$$[\Phi] = \frac{1}{j\omega}[P^C][I^{C_{\text{Dis}}}] + \frac{1}{j\omega}[P^D][I^{D_{\text{Dis}}}] \tag{70}$$

where $[L]$ is the inductance matrix defined by (66), $[C]$ is the capacitance matrix defined by (60), $[K^{CC}]$ is the CCCS matrix defined by (62), $[K^{CV}]$ is the CCVS matrix defined by (57), $[P^{C(D)}]$ is the potential coefficient matrices defined by (54) and (55), $[I^{C(D)}]$ is the vectors of surface currents, $[\phi]$ is the vector of node potentials, $[\delta V^{C(D)}]$ is the vectors of voltages between two adjacent nodes, $[I^{C(D)_{\text{Dis}}}]$ is the vectors of displacement currents, $[V^D]$ is the vector of surface voltage on dielectric surfaces, and $[V_S]$ is the voltage excitation vector.

The superscripts of C and D of the coupling matrices in (67)–(70) stand for conductors and dielectrics, respectively. The vector of displacement current $[I^{C(D)_{\text{Dis}}}]$ is related to surface current vector $[I^{C(D)}]$ by KCL equation

$$[I^{C(D)_{\text{Dis}}}] = [A^{C(D)}][I^{C(D)}] \tag{71}$$

where $[A^{C(D)}]$ is connectivity matrix. Entry A_{ij} in matrix $[A^{C(D)}]$ is 1 or -1 if the current on the jth current mesh flows into or out of the ith charge mesh, otherwise is 0.

In summary, the proposed S-PEEC model for a general quasi-static EM problem involving dielectrics and conductors can be obtained in the circuit form shown in Fig. 6. The PEEC representing conductors is in consistent with that of the conventional S-PEEC model and that for dielectrics the dominant circuit element is the self-capacitance. In the PEEC model shown in Fig. 6, couplings among different types of circuit elements are represented by different symbols: a triangular dot stands for inductive coupling among conductor current cells, a circular dot refers to capacitive coupling among all the charge cells, and capacitive coupling between dielectric surface current cells is represented by a square dot. The influence of electric current on conductor surfaces to dielectric surfaces is represented by controlled sources. In conclusion, the circuit for the conductors couples to that for dielectrics through two mechanisms: 1) the controlled voltage and current sources on dielectric surfaces by the current on conductor

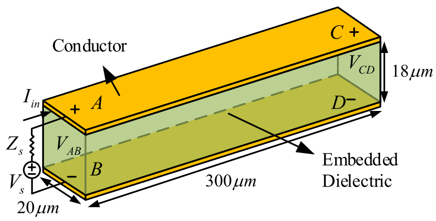

Fig. 7. Geometry of transmission line structure.

surfaces and 2) the capacitive coupling among the displacement currents on the surfaces of conductors and dielectrics. Since the number of circuit elements on dielectric surfaces in the proposed PEEC model is $M_d^2 + N_d^2$, compared with $4M_d^2 + 2N_d^2$ elements in the conventional S-PEEC model, the simulation time and required memory of the proposed PEEC model is reduced significantly.

V. Numerical Examples

To validate the accuracy and effectiveness of the proposed PEEC model, three numerical examples are investigated. Triangular meshes and RWG basis functions [17] are adopted in all the examples. modified node analysis [18] is used to analyze the PEEC models for obtaining the S-parameters. A transmission line [3], an LTCC component and a multilayer interconnection circuit are given in this section. The results in the frequency domain by the proposed model are compared with those by S-PEEC and commercial software. Same mesh scheme is used by the proposed PEEC and the S-PEEC in each of the examples. A time-domain transient analysis is given in example 1 to demonstrate the applicability of the proposed PEEC model for time-domain analysis.

A. Example 1: Transmission Line of Finite Dielectric

A transmission-line structure as shown in Fig. 7, which is an example in [3], is first analyzed using the proposed PEEC model. The thickness of the conductor traces are set to be 0.1μm. The dielectric block is 18 μm thick, 20 μm wide, and 300 μm long. The transmission line is excited by a 1-V voltage source at one end. The frequency-domain responses of the imaginary part of input current I_{in} through the voltage source are shown in Fig. 8(a). Compared with the results of HFSS and the S-PEEC model in [3] for relative dielectric constants (ε_r) of 10 and 20, good agreement is observed. It can also be seen that the resonance frequency shifts with the change in dielectric constant. A comparison between the attributes and computational overhead of the conventional S-PEEC and the proposed PEEC is given in Table II. It is noticed that the numbers of branches and nodes are reduced nearly by half in the proposed PEEC model. The number of coupling elements is also reduced significantly. As the problem under the quasi-static assumption, the radiation effect is not considered in the proposed PEEC mode. Therefore, the real part of I_{in} is constantly equals to zero.

To valid the proposed model for time-domain simulation, the transmission line structure with $\varepsilon_r = 10$ is excited by

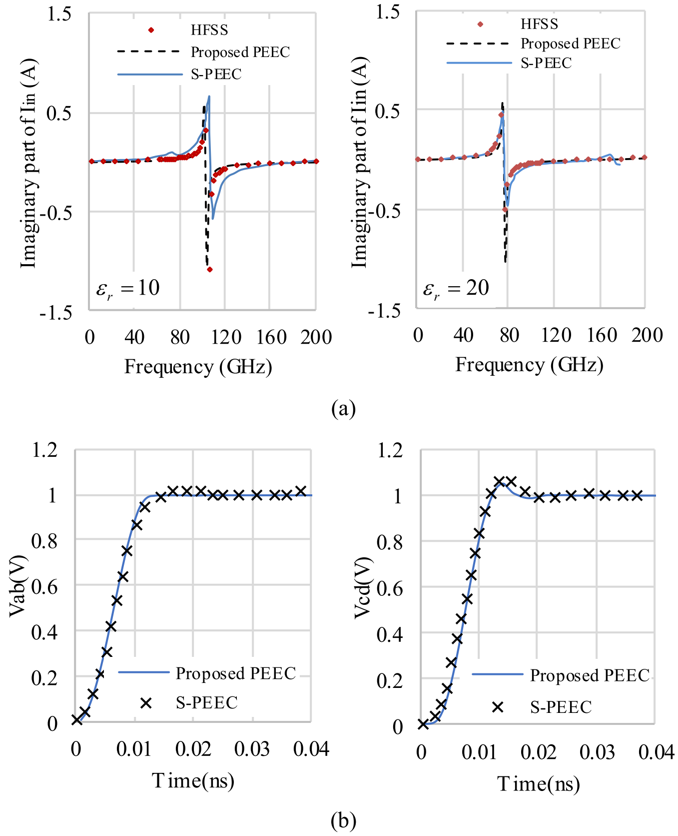

Fig. 8. (a) Imaginary part of current through voltage source for relative permittivity of 10 and 20. (b) Time-domain responses of V_{AB} and V_{CD} for relative permittivity of 10.

TABLE II
Circuit Size and Computing Time of the Proposed PEEC Model and the Conventional S-PEEC Model

	Proposed PEEC	Conventional S-PEEC
No. of nodes	892	1,420
No. of branches	1,258	2,050
No. of inductive couplings	217,156	2,209,828
No. of capacitive couplings	627,264	0
No. of potential couplings	795,664	1,074,448
No. of controlled source couplings	369,072	1,992,672
No. of Unknowns	2,943	3,470
S-Parameters simulation time	1 min 22s	2 min 29 sec

voltage source V_s with a sin-square waveform, whose magnitude is 1 V and raise time is 9.5 ps. As shown in Fig. 7, V_s is connected in series with a 10-Ω source resistor Z_S between points A and B. The other end is left open. The simulated voltages V_{AB} and V_{CD}, which are the potential differences between points A and B and points C and D, respectively, are plotted in Fig. 8(b). The results are validated by those obtained in [3] by S-PEEC model, showing very good agreement.

B. Example 2: LTCC Filter Component

The second example is a typical LTCC bandpass filter component shown in Fig. 9. The filter is embedded in an

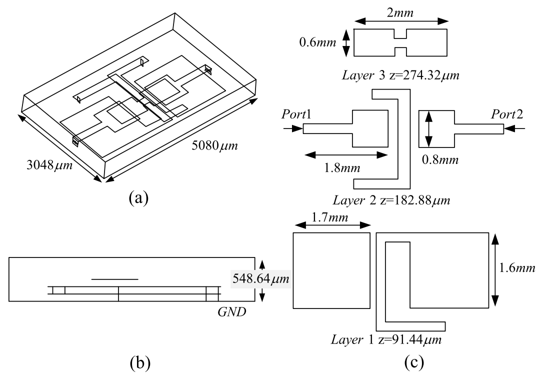

Fig. 9. LTCC bandpass filter. (a) Isometric view. (b) Side view in the *yz* plane. (c) Top view of each layer in the *xy* plane and its brief physical dimensions.

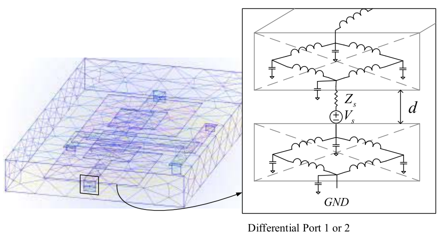

Fig. 10. Mesh scheme of the LTCC filter and port definition.

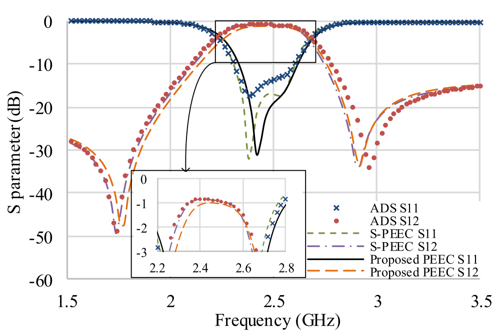

Fig. 11. Comparison of the numerical results by the proposed PEEC model, S-PEEC, and agilent ADS momentum.

electrically small dielectric block with relative permittivity $\varepsilon_r = 7.8$ and thickness of each layer is 91.44 μm. The resistivity of conductor strips is set to 10^{-8} $\Omega\cdot$m. The definition of the differential ports is illustrated in Fig. 10. Since the bottom surface is the ground plane, two electrode pads are added to each port with a small gap in the middle for applying a delta-gap voltage source [19]. In the circuit domain, the nodes on the two charge meshes besides the gap are connected by a voltage source in series with a reference resistor whose value equals to the port impedance as shown in Fig. 10. The surfaces of the conductor and dielectrics are divided into 1339 meshes. The number of nodes in the circuit domain of the proposed PEEC and S-PEEC is 1339 and 2071, respectively. In Fig. 11, the magnitude of S-parameters calculated by the proposed PEEC model, commercial EM software ADS momentum [9], and the traditional S-PEEC model are compared. Good agreement is observed.

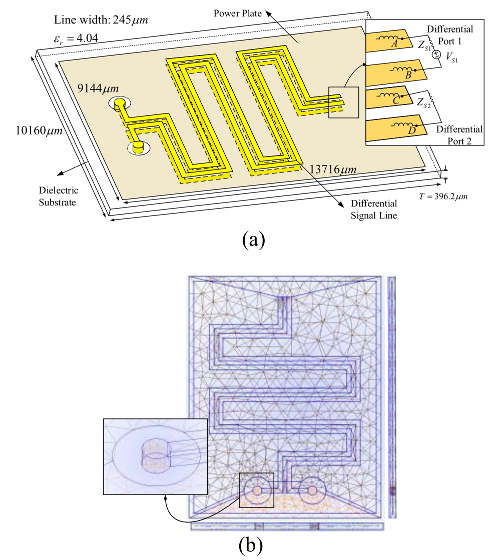

Fig. 12. (a) Circuit layout of a multilayer interconnection circuit with through vias and a pair of differential signal lines (with port excitation enlarged). (b) Mesh scheme (with meshes around a via are enlarged).

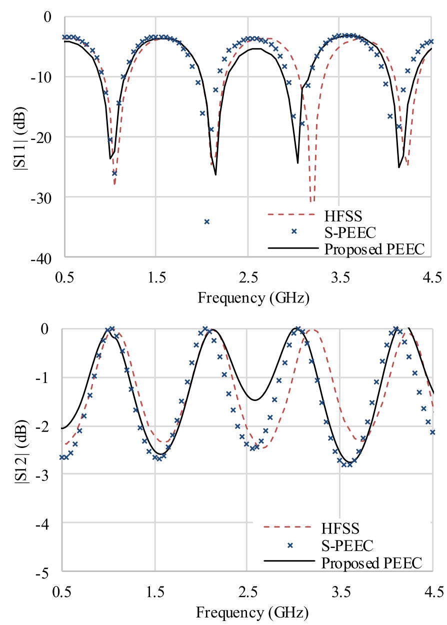

Fig. 13. Magnitude of S-parameters calculated by HFSS, S-PEEC, and the proposed PEEC model.

C. Example 3: Multilayer Interconnection Circuit

To valid the ability of the proposed method to model an interconnection problem, a typical multilayer interconnection circuit with through via holes and a pair of differential signal lines is studied. The physical geometry and the excitation method of the circuit board are shown in Fig. 12(a). In the circuit, there is a layer of power plate and two layers of signal traces, which are connected by a pair of via holes embedded in the substrate with dielectric constant of 4.04. The conductor strips are treated as a 3-D perfect conductor block with thickness of 1 μm. The thickness of the dielectric substrate is 396.2 μm and the traces are located at the top and bottom surfaces of the substrate. Two delta-gap voltage sources are applied at the ports of the traces. The other dimensions are given in Fig. 12(a). As shown in Fig. 12(b), 2774 meshes are employed to construct the conductor and dielectric surfaces. It also can be observed that the triangular meshes fit the via hole structures well. The number of nodes in the circuit domain of proposed PEEC and S-PEEC is 2774 and 4306, respectively. As shown in Fig. 13, good agreement is observed in the frequency range below the second resonance compared with the results of HFSS and traditional S-PEEC. Above the second resonance frequency, the response deviates from HFSS's result slightly due to the quasi-static assumption.

VI. Conclusion

In this paper, a quasi-static S-PEEC model is presented for modeling EM problems involving conductors and heterogeneous dielectrics of finite size. The new PEEC model is based on three integral equations, namely, EFIE for conductors, MFIE, and EFIE for dielectrics, under quasi-static assumption. The new set of integral equations allow the PEEC model describing dielectric surfaces only contains capacitive coupling and controlled sources that reflect the coupling with the subcircuit for conductors, leading to a significant size reduction of the subcircuit for describing dielectrics compared to the full-wave S-PEEC model. The new PEEC model provides a frequency-invariant lumped element circuit for a general EM problem under quasi-static assumption. The proposed PEEC model is proved to be suitable for both the frequency- and time-domain analysis. The model will be particularly useful for practical packaging and interconnection problems in which the electrical size is relative small.

References

[1] A. E. Ruehli, "Equivalent circuit models for three-dimensional multiconductor systems," *IEEE Trans. Microw. Theory Techn.*, vol. 22, no. 3, pp. 216–221, Mar. 1974.

[2] A. E. Ruehli and H. Heeb, "Circuit models for three-dimensional geometries including dielectrics," *IEEE Trans. Microw. Theory Techn.*, vol. 40, no. 7, pp. 1507–1516, Jul. 1992.

[3] D. Gope, A. E. Ruehli, C. Yang, and V. Jandhyala, "(S)PEEC: Time- and frequency-domain surface formulation for modeling conductors and dielectrics in combined circuit electromagnetic simulations," *IEEE Trans. Microw. Theory Techn.*, vol. 54, no. 6, pp. 2453–2464, Jun. 2006.

[4] A. E. Ruehli, G. Antonini, J. Esch, J. Ekman, A. Mayo, and A. Orlandi, "Nonorthogonal PEEC formulation for time- and frequency-domain EM and circuit modeling," *IEEE Trans. Electromagn. Compat.*, vol. 45, no. 2, pp. 167–176, May 2003.

[5] A. E. Ruehli and A. C. Cangellaris, "Progress in the methodologies for the electrical modeling of interconnects and electronic packages," *Proc. IEEE*, vol. 89, no. 5, pp. 740–771, May 2001.

[6] J. Jayabalan, B.-L. Ooi, M.-S. Leong, and M. K. Iyer, "Novel circuit model for three-dimensional geometries with multilayer dielectrics," *IEEE Trans. Microw. Theory Techn.*, vol. 54, no. 4, pp. 1331–1339, Jun. 2006.

[7] J. Wang and K.-L. Wu, "A derived physically expressive circuit model for multilayer RF embedded passives," *IEEE Trans. Microw. Theory Techn.*, vol. 54, no. 5, pp. 1961–1968, May 2006.

[8] H. Hu, K. Yang, K. L. Wu, and W. Y. Yin, "Quasi-static derived physically expressive circuit model for lossy integrated RF passives," *IEEE Trans. Microw. Theory Techn.*, vol. 56, no. 8, pp. 1954–1961, Aug. 2008.

[9] Y. Dou and K.-L. Wu, "Direct mesh-based model order reduction of PEEC model for quasi-static circuit problems," *IEEE Trans. Microw. Theory Techn.*, vol. 64, no. 8, pp. 2409–2422, Aug. 2016.

[10] Y. Dou and K.-L. Wu, "A passive PEEC-based micromodeling circuit for high-speed interconnection problems," *IEEE Trans. Microw. Theory Techn.*, vol. 66, no. 3, pp. 1201–1214, Mar. 2018.

[11] C. Liao, Z. Zhu, Q. Lu, X. Liu, and Y. Yang, "Wideband electromagnetic model and analysis of shielded-pair through-silicon vias," *IEEE Trans. Compon., Packag. Manuf. Technol.*, vol. 8, no. 3, pp. 473–481, Mar. 2018.

[12] M. Friedrich and M. Leone, "Quasi-static inductance of vertical interconnections in parallel-plane structures," *IEEE Trans. Electromagn. Compat.*, vol. 54, no. 6, pp. 1302–1305, Dec. 2012.

[13] J. Siau, G. Meunier, O. Chadebec, J.-M. Guichon, and R. Perrin-Bit, "Volume integral formulation using face elements for electromagnetic problem considering conductors and dielectrics," *IEEE Trans. Electromagn. Compat.*, vol. 58, no. 5, pp. 1587–1594, Oct. 2016.

[14] D. Romano and G. Antonini, "Quasi-static partial element equivalent circuit models of linear magnetic materials," *IEEE Trans. Magn.*, vol. 51, no. 7, pp. 1–15, Jul. 2015.

[15] J. Van Bladel, *Electromagnetic Fields*, 2nd ed. New York, NY, USA: Wiley, 2007, pp. 189–191 and 624–625.

[16] A. E. Ruehli and P. A. Brennan, "Efficient capacitance calculations for three-dimensional multiconductor systems," *IEEE Trans. Microw. Theory Techn.*, vol. MTT-21, pp. 76–82, Feb. 1973.

[17] S. M. Rao, D. R. Wilton, and A. W. Glisson, "Electromagnetic scattering by surfaces of arbitrary shape," *IEEE Trans. Antennas Propag.*, vol. AP-30, no. 3, pp. 409–418, May 1982.

[18] C.-W. Ho, A. E. Ruehli, and P. A. Brennan, "The modified nodal approach to network analysis," *IEEE Trans. Circuits Syst.*, vol. CAS-22, no. 6, pp. 504–509, Jun. 1975.

[19] G. V. Eleftheriades and J. R. Mosig, "On the network characterization of planar passive circuits using the method of moments," *IEEE Trans. Microw. Theory Techn.*, vol. 44, no. 3, pp. 438–445, Mar. 1996.

Yang Jiang received the B.S. degree in electronics engineering from The Chinese University of Hong Kong, Hong Kong, in 2013, where he is currently pursuing the Ph.D. degree.

His current research interests include partial element equivalent circuit (PEEC) modeling, full-wave circuit domain modeling for signal integrity and electromagnetic compatibility problems, and compact PEEC model for electromagnetic problems with inhomogeneous dielectrics in both the frequency and time domains.

Ke-Li Wu (M'90–SM'96–F'11) received the B.S. and M.Eng. degrees from the Nanjing University of Science and Technology, Nanjing, China, in 1982 and 1985, respectively, and the Ph.D. degree from Laval University, Quebec, QC, Canada, in 1989.

From 1989 to 1993, he was a Research Engineer with McMaster University, Hamilton, ON, Canada. In 1993, he joined the Corporate Research and Development Division, COM DEV (now Honeywell Aerospace), Cambridge, ON, Canada, where he was a Principal Member of Technical Staff. Since 1999, he has been with The Chinese University of Hong Kong, Hong Kong, where he is currently a Professor and the Director of with the Radio Frequency Radiation Research Laboratory. His current research interests include EM-based circuit domain modeling of high-speed interconnections, robot automatic tuning of microwave filters, decoupling techniques of multi-in multi-out antennas, and Internet of Things technologies.

Dr. Wu is a member of the IEEE MTT-8 Subcommittee. He serves as a TPC member for many prestigious international conferences. He was a recipient of the 1998 COM DEV Achievement Award and the Asia–Pacific Microwave Conference Prize in 2008 and 2012. He was an Associate Editor of the IEEE Transactions on Microwave Theory and Techniques from 2006 to 2009.